PNAS

Supporting Information for

Solvation-induced local structure in liquids probed by high-harmonic spectroscopy

Eric Moore, Sucharita Giri, Andreas Koutsogiannis, Tahereh Alavi, Greg McCracken, Kenneth Lopata, John M. Herbert, Mette B. Gaarde, and Louis F. DiMauro

Louis DiMauro.
E-mail: dimauro.6@osu.edu

This PDF file includes:

Supporting Information Text

Experimental Apparatus. See Figure S1 and discussion in Methods.

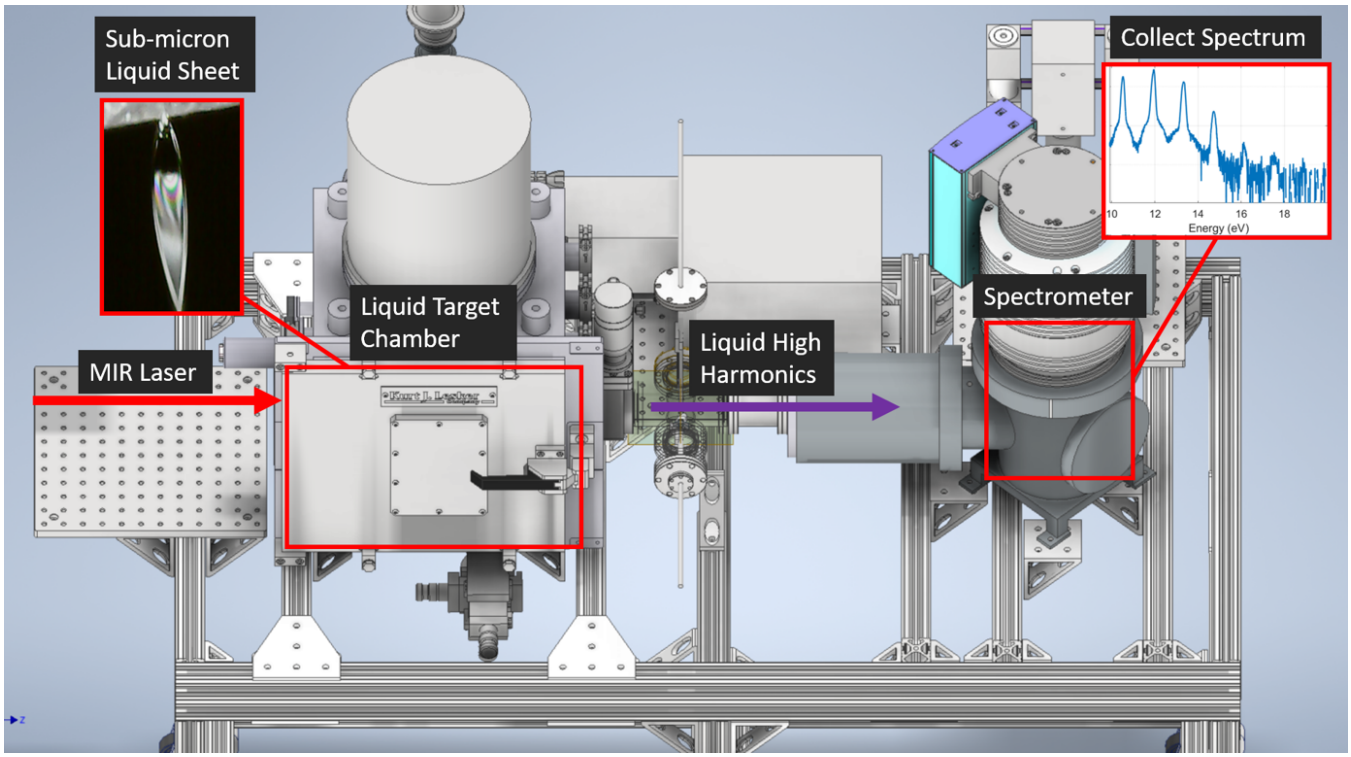

Fig. S1. The vacuum apparatus used in the experiments. The laser pulses enter the liquid target chamber through a CaF_2 window located on the left and are focused onto the ultra-thin liquid sheet using a 30 cm focal length, anti-reflective coated lens. The generated harmonic light then propagates down to a spectrometer where the light is collected on an MCP/phosphor detector and imaged on a CMOS camera.

Binary Solutions: Choice of Solute and Solvent. Our final choice of binary solutions presented in this manuscript were preceded by a systematic characterization of several neat liquids which would satisfy both fundamental and practical criteria. At the most simplistic level of consideration is whether the liquid itself will emit high harmonics and with what strength? Second, what are the physical and chemical properties of each, and which liquids are compatible? The following highlights some of the rationale.

General Strategy: To optimize the detection sensitivity of the more dilute solute in a solvent, we targeted molecular solutes that had much brighter harmonic emission compared to the solvent at the same intensity. One criterion, we choose a solute molecule ($\leq$ 8 eV) with a lower ionization potential than the molecular solvent ($\geq$ 9.5 eV).

Solvent Evaluation: In our study, we have (1) characterized the harmonic emission from methanol, ethanol, and water in our apparatus. (2) For technical reasons, in general, alcohols work best in the liquid jet set-up since they have a very low melting point and an ideal viscosity. (3) Alcohols are polar solvents, providing a better opportunity to observe effects resulting from differing solute-solvent interaction dependence on the solutes polarity. Thus, in terms of choosing a solvent for solvent-solute studies alcohols are an ideal candidate and in particular, methanol is dominated by its polar component.

Solute Evaluation: Given the points above, (1) we require solutes that readily dissolve in solution across a broad range of concentration. Both benzene and halo-benzenes are soluble in methanol and significantly less so in water. (2) Benzene and its derivatives are known to be very bright emitters both in gas phase and liquid phase, even at low laser intensity. This maximizes our opportunity to observe solute harmonics and any effects from solute-solvent interaction. (3) Halo-benzenes have a significant polarity, and so we can observe the effects of polar interactions in methanol. Toluene provides a non-polar reference solute.

Identification of High Harmonics from Solution and Gas-Phase. There are several experimental observations that clearly differentiate and control the harmonic emission from liquid and gas phase molecules. Furthermore, our liquid HHG observation are consistent with prior reports by the Wörner group (see main text Refs. 4–6).

Under our typical operation condition, our liquid sheet is approximately 100 microns at its widest point with a thickness ranging from 0.1-1 microns. Typical operational values are 300-400 nm thickness. An imaging system monitors the position of the laser focus relative to the transverse/longitude position of the sheet and an in-situ interferometer measures the sheet thickness. The entire nozzle assembly can be translated while the laser focus is kept fixed for alignment with the downstream XUV spectrometer.

Using different liquids and laser conditions, we performed several investigations that observe the HHG spectrum as the laser focus is moved transversely "in" the sheet and "off" the sheet edge. Here we assume that "off" the sheet only gas-phase molecules are present. Figure S2 presents the HHG spectrum "on" (liquid) and "off" (gas) the sheet for two different laser intensities. Several things are evident; the gas-phase produces higher-order harmonics compared to the liquid and the linewidth of the gas harmonics are narrower. In addition, moving "off" the sheet the observed gas-phase harmonic emission is significantly weaker than the liquid consistent with a reduction in the density.

Another unique signature of liquid harmonic emission is the nearly independent behavior of the HHG cutoff energy on the laser parameters. This is evident in Figure 2A and Figure S2 where the "in" sheet liquid harmonic cutoff energy is fixed (12—14 eV) and independent of the intensity while the "off" sheet gas-phase harmonic cutoff energy increases linearly with intensity. This is further illustrated in Figure S3 where the liquid harmonic cutoff energy remains fixed even though the laser wavelength is varied by a factor of two. This is in disagreement with the well-known λ^2-scaling law (1) of the cutoff energy in gas-phase harmonic generation and instead illustrates the unique property of the length-scale indicative liquid-phase harmonics.

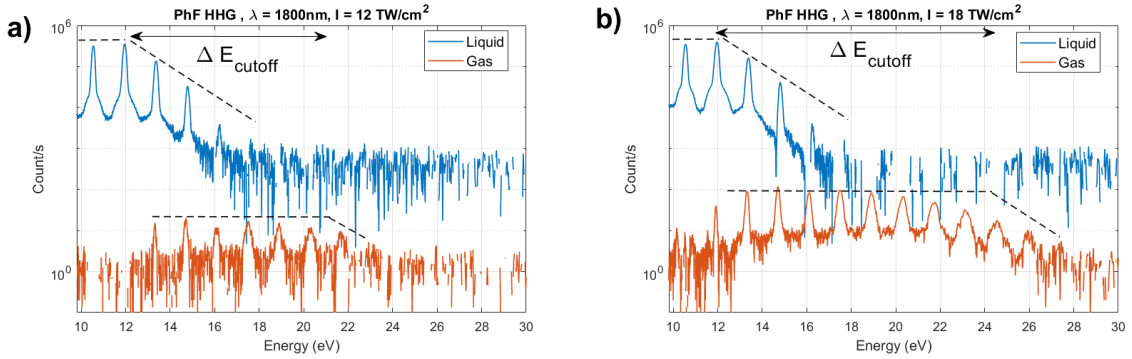

Fig. S2. High harmonic emission from liquid (blue) and gas-phase (red) PhF taken at the same intensity for two different values (a) 12 and (b) 18 TW/cm^2. The spectra are recorded using the liquid sheet translation method described above. Note, that the gas-phase PhF has a higher cutoff energy with increasing intensity while the liquid cutoff is lower and unchanged. Also notice the large decrease ($10-4$) in the emission strength for the rarified PhF gas compared to the brighter liquid.

Wavelength Independent Harmonic Cutoff Energy. As recently observed by Mondal *et al.*, high harmonic spectra generated from neat liquid water and ethanol exhibit a cutoff energy essentially independent of wavelength over the range of 800-1800 nm, in stark contrast to the quadratic wavelength dependence observed in gas phase HHG (2). Likewise, they observed a weak solvent dependent shift in the cutoff energy. Our measurements agree with their observations but expands the wavelength range to 3200 nm and other solvents, i.e. PhF, toluene, difluoro- and hexa-fluorobenzene, and other halogenated-benzene derivatives. In all cases, the liquids manifest a cutoff energy in the 12-16 eV range, indicative of the importance of the length-scale in defining the electron dynamics. In addition, Supplementary Figure S3 shows that the cutoff energy of liquid toluene remains independent of the driving wavelength even though the wavelength changes by a factor of two (1600 - 3200 nm). Concurrent measurements of gas-phase toluene, and other molecules, show the expected λ^2-scaling.

Harmonic Suppression Dependence on Wavelength. Supplementary Figure S4 shows the variation of the harmonic spectrum with wavelength for a fixed concentration of 9% PhF in methanol and constant intensity (22 TW/cm^2). As shown in the figure, as the laser wavelength is finely varied from 1700 nm to 2000 nm in 20 nm steps the harmonic energy and spacing changes accordingly. Most interestingly, the amount of suppression of the 17^{th}-order harmonic also changes, thus sampling the spatial extent of the structure at some mean distance.

Other Fluorinated Benzene Derivatives. In order to fully explore the role of fluorine in the high harmonic process, we studied the series of difluorobenzene in methanol, namely ortho (1,2), meta (1,3) and para (1,4). Supplementary Figure S5 shows the harmonic spectra for each at 9% molar concentration of difluorobenzene and compares with the pure liquids. Also plotted on the panels to the right are the harmonic yield ratios of each solution compared to pure methanol. In all cases, the difluoro derivatives show a similar overall reduction in emission in the plateau region compared to that of PhF, with the largest suppression occurring for the ortho-difluorobenzene. However, the difluoro derivatives do not show an order-dependent suppression that is so evident in PhF. Nonetheless, the general trend suggests that the inclusion of fluorine plays a role in its interaction with the methanol environment.

Effect of the Repulsive Barrier Shape on the Harmonic Spectrum. In Supplementary Figure S6, we present the calculated HHG spectra for several different combinations of height (N) and width (σ) of the repulsive potential barriers defined in Methods. In the left (right) panel, all the barriers are positioned at the same central location of 4.65 Å(5.5 Å), to maximally suppress harmonic 13 (19). To enhance visualization, the intensity of each spectrum is offset by a value of 3 on a logarithmic scale. These results show that the observed suppression of a specific harmonic order is quite robust for different heights and widths of the barrier, and that lowering the barrier (larger N) can generally be compensated by increasing the width (larger σ).

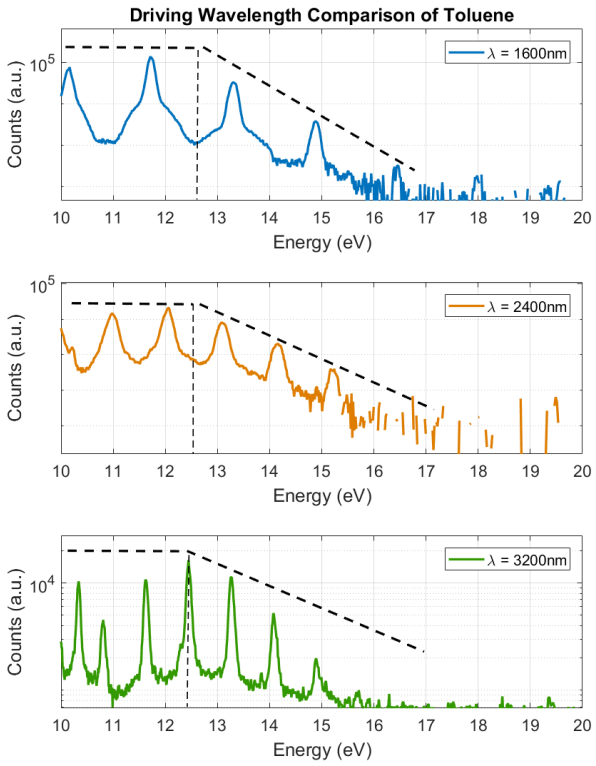

Fig. S3. Measured harmonic spectra from liquid toluene at three different driving wavelengths. The laser intensity for all three wavelengths is 20 TW/cm^2. The cutoff energy is indicated by the dashed vertical line. The spectral feature in the 3200 nm plot at around 10.4 eV is a plasma line emission which is also weakly visible at the same spectral energy in the 2400 nm plot.

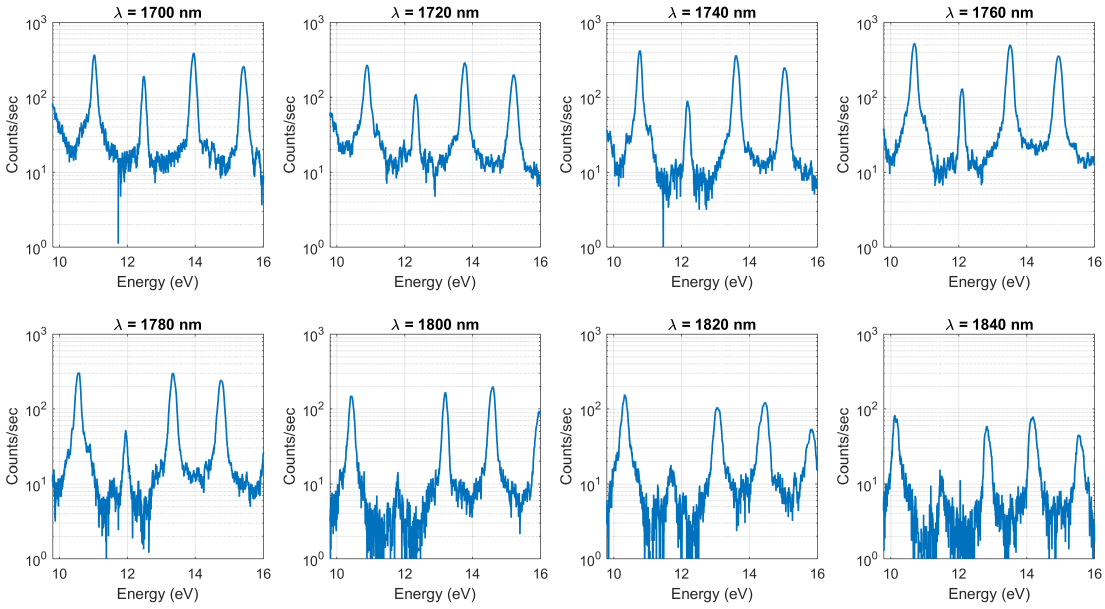

Fig. S4. Measured harmonic spectra as a function of wavelength from 1700 to 1840 nm for a 9% PhF in methanol solution.

Illustration of Suppression Mechanism in 1D TDSE Model. We illustrate the mechanism for harmonic suppression in the 1D TDSE model in Figure S7, showing time-frequency maps of the harmonic response calculated for a laser pulse with a wavelength

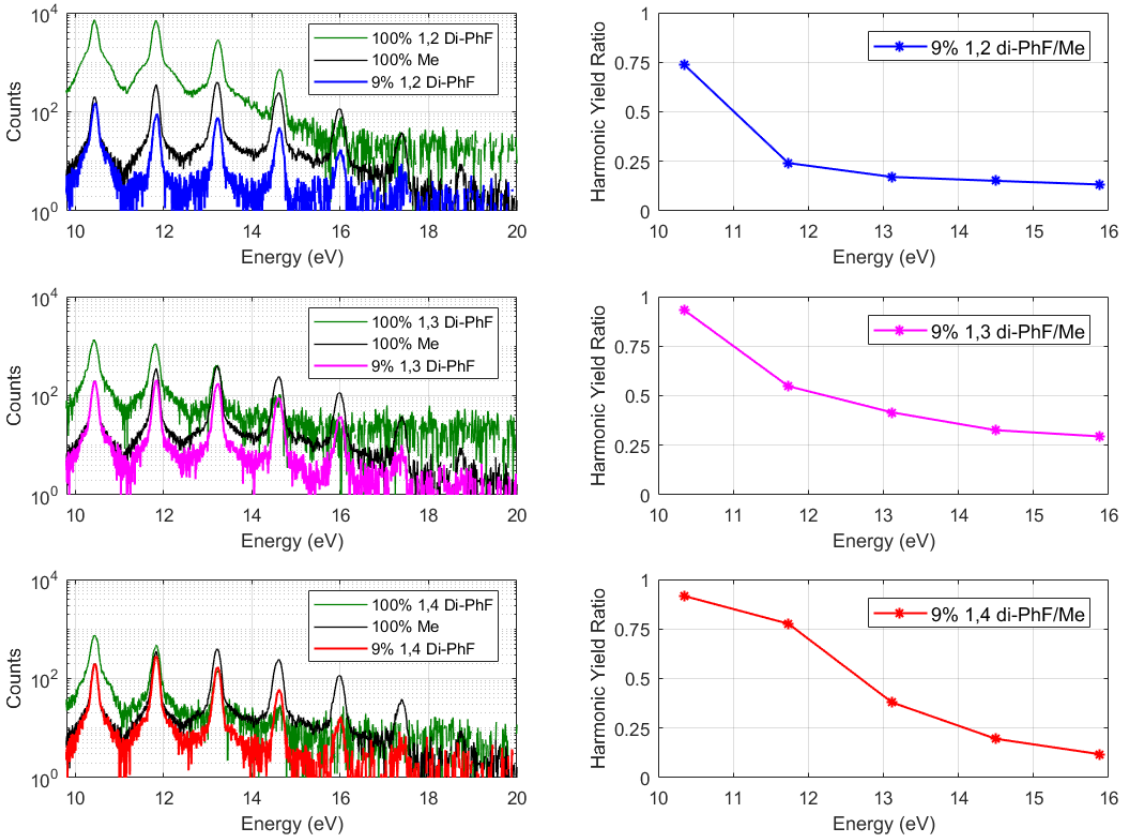

Fig. S5. Left side: The HHG spectra of three 9% molar solutions of DiPhF isomers (1,2 (blue), 1,3 (pink), 1,4 (red)) solvated in methanol along with spectra from pure methanol (black) and pure DiPhF isomers (green) for reference. Right side: ratio of the harmonic yield of the solution to pure methanol. All spectra were taken under the same laser and sheet conditions using a wavelength of 1800 nm and intensity of 25 TW/cm^2.

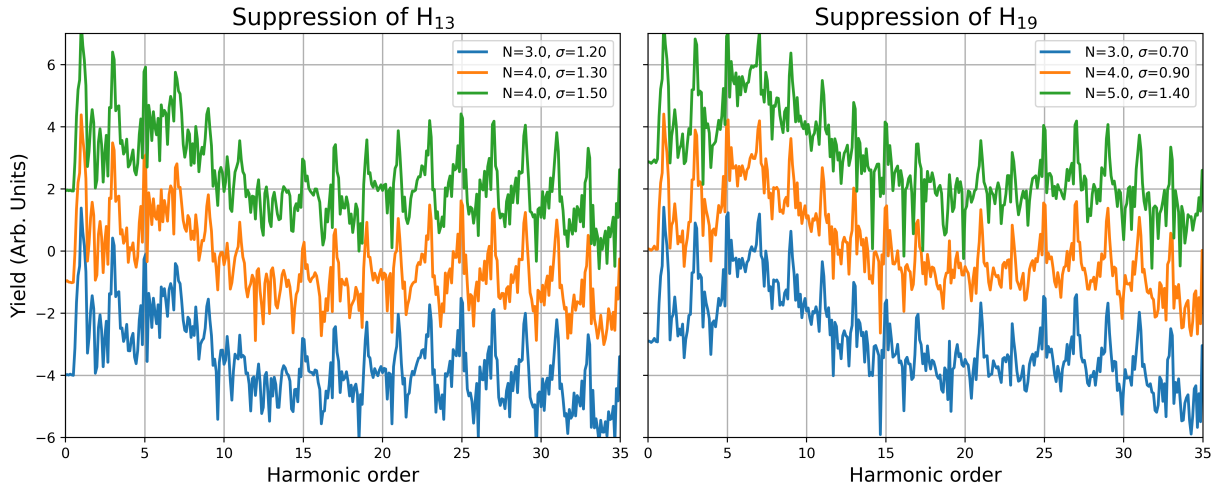

Fig. S6. HHG spectra are plotted for various barrier heights and widths positioned at 4.65 Å (left, for suppression of harmonic 13), and 5.50 Å (right, harmonic 19) using a laser pulse with a wavelength of 1800 nm and an intensity of 20 TW/cm^2.

of 1800 nm and an intensity of 20 TW/cm^2. The left-hand side has no repulsive barrier and the right-hand side has the barrier in the position that maximally suppresses harmonic 19 (5.5 Å). In both calculations, an absorbing boundary lowers the cutoff energy from H42 (as predicted by the isolated-atom cutoff law (3)) to approximately H27. The absorbing boundary starts

at 8 Å and slowly suppresses the wavefunction over 32 Å to avoid artificial reflections on the boundary. The left-hand side shows that in addition to lowering the cutoff energy, the absorbing boundary has the effect of completely eliminating the long trajectory contributions to the HHG yield. The right-hand side shows the effects of adding the repulsive barrier: All the harmonics in the plateau region are strongly suppressed by the interaction with the barrier, but there is a range of harmonics between approximately 15 and 20 that are suppressed even further. We note that these harmonics are not substantially shifted in their emission times and are still consistent with suppression of the no-barrier short trajectories. In addition, the barrier facilitates a weaker family of trajectories that return almost a half-cycle later for H19 and cause destructive interference. When we track the evolution of the time-frequency plots with the position of the barrier, we see both of these effects consistently: a weakening of the short trajectory contribution itself, and a new class of later-return trajectories that return at different times for different barrier locations, thus leading to destructive interference of different harmonics.

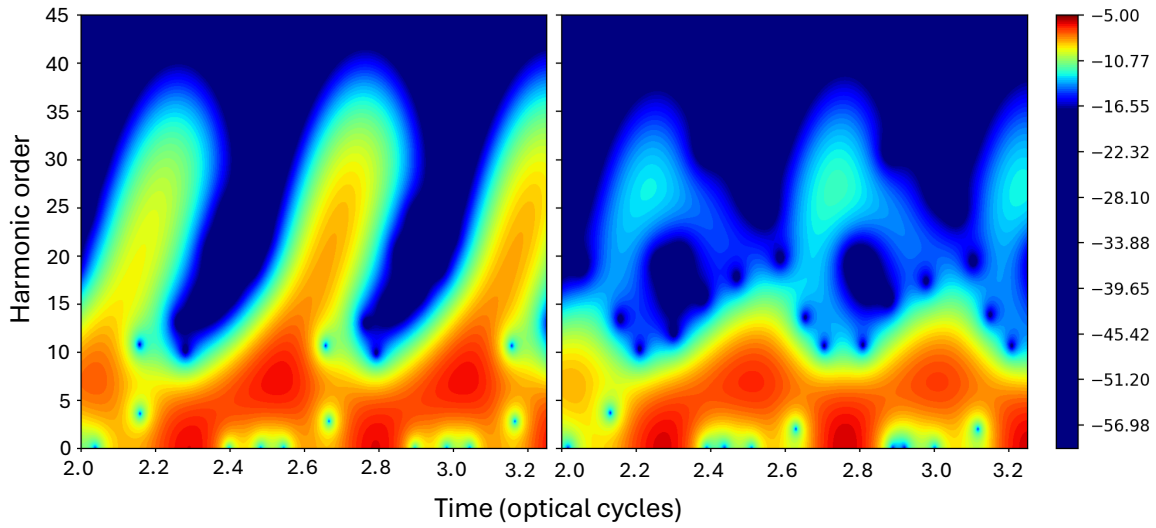

Fig. S7. Time-frequency map for the HHG spectra are plotted for without (left) and with (right) the repulsive barrier, using a laser pulse with a wavelength of 1800 nm and an intensity of 20 TW/cm^2.

Concentration Dependence of MD simulation of PhF-MeOH Mixture. Figure S8 shows MD calculations of the site–site (fluorine to hydroxyl hydrogen) radial distribution function (RDF) for the four 9% concentrations of PhX in 91% MeOH (same as Fig. 5 in main text), with an added curve for the RDF of a 14% PhF in 86% MeOH. There is no meaningful shift of the position of the PhF...HOCH3 hydrogen bond between the two concentrations, although the 14% curve has a slightly lower peak value.

References

1. ATMHGSPAP Tate, J., LF DiMauro, Scaling of wave-packet dynamics in an intense midinfrared field. *Phys. Rev. Lett.* **98**, 013901 (2007).
2. A Mondal, et al., High-harmonic generation in liquids with few-cycle pulses: effect of laser-pulse duration on the cut-off energy. *Opt. Express* **31**, 34348–34361 (2023).
3. K Schafer, B Yang, L DiMauro, K Kulander, Above threshold ionization beyond the high harmonic cutoff. *Phys. Rev. Lett.* **70**, 1599 (1993).

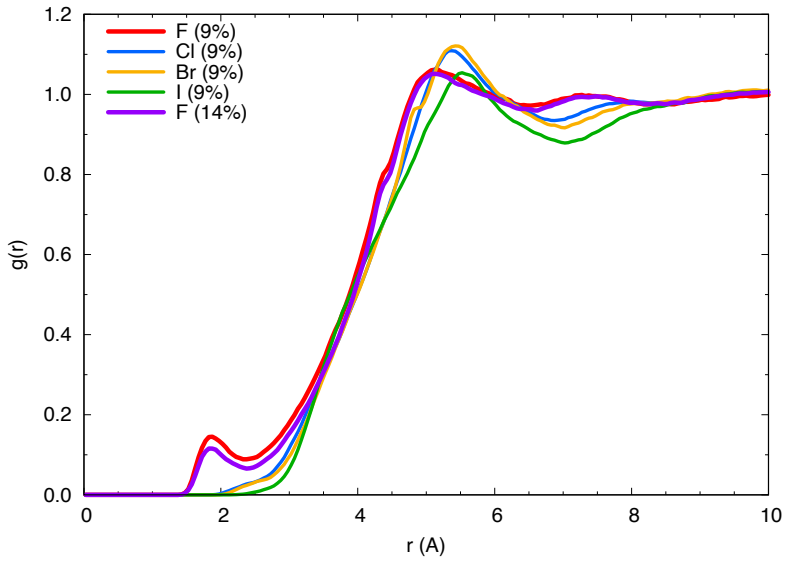

Fig. S8. Site–site (halogen to hydroxyl hydrogen) RDF for a 9% (by mole) PhX solution in 91% MeOH, with X = F, Cl, Br, or I (same as Fig. 5 in main text), with an added curve for a 14% PhF solution in 91% and 86% MeOH.